Thermal transmittance of a composite lightweight wall panel with integrated load-bearing structure: Experimental versus numerical approach

Gaši, Mergim; Milovanović, Bojan; Tkalčić, Domagoj; Jelčić Rukavina, Marija

Case Studies in Construction Materials 19 (2023) e02631

Contents lists available at ScienceDirect

Case Studies in Construction Materials

journal homepage: www.elsevier.com/locate/cscm

Case study

Thermal transmittance of a composite lightweight wall panel with integrated load-bearing structure: Experimental versus numerical approach

Mergim Gaši *, Bojan Milovanović, Domagoj Tkalčić, Marija Jelčić Rukavina

Department of Materials, Faculty of Civil Engineering, University of Zagreb, Croatia

ARTICLE INFO

Keywords:
Lightweight steel structures
Thermal transmittance
Experimental measurements
Numerical simulations
U-values
Heatflow method

ABSTRACT

One of the most important parameters when it comes to heat losses in buildings is the thermal transmittance or U-value. Therefore, great importance should be given to the determination of U-values, especially for elements where there is a high thermal bridge effect, as is the case with lightweight steel frame (LSF) structures. Since LSF structures are usually geometrically more complex, especially when diagonal elements are present, the determination of the overall U-value of these elements is usually done either on scale models in the laboratory or by numerical methods. This paper compares different methods for determining the total U-value for four different polyurethane foam-filled LFS walls and a reference wall made of EPS. Analytical (ISO 6946), experimental (Guarded Hot Box Method and HFM) and numerical 2D and 3D calculations were used to determine the U-value. The aim of the comparison was to verify which methods can be used for more complex geometries of LSF walls when there is a stronger influence of point thermal bridges due to the additional diagonal bracing. All methods showed similar U-values with the highest absolute deviation of 17.18% between the HFM and the 3D numerical calculations. The analytical method for inhomogeneous building elements given in ISO 6946 agrees well with all methods with the maximum absolute deviation of 8.83% between the analytical and HFM method. The work showed the importance of the placement of the HFM sensor for the determination of the surface heat flux, as incorrect placement of the sensor can result in inadequate U-values that deviate up to 167% from the true value.

1. Introduction

Recently, the focus has largely been on sustainability, reducing CO_2 emissions, and improving energy efficiency. Approximately 40% of the total energy consumption and 36% of CO2 emissions can be attributed to the building sector [1]. The European Union has a large number of buildings that are over 50 years old, and unfortunately, many of these buildings are not energy efficient. [2]. To reduce these statistics, the European Union has issued a directive stating that starting from 2019, all public buildings must meet near-zero energy building (nZEB) standards, and from 2021 onwards, all new buildings must be constructed as nZEBs [3].

In order to align EU policies with the climate goals established by the Council and the European Parliament, the Fit for 55 package was introduced [4]. This comprehensive plan includes various measures aimed at reducing CO2eq emissions from buildings by 2030

* Corresponding author.
E-mail address: mgasi@grad.hr (M. Gaši).

https://doi.org/10.1016/j.cscm.2023.e02631
Received 26 June 2023; Received in revised form 27 September 2023; Accepted 29 October 2023
Available online 2 November 2023

compared to 2005. The proposed actions involve improving energy performance of new and renovating existing buildings to enhance their energy performance. These initiatives are in line with the European Commission's long-term plan to create a low-carbon Europe by 2050 [5,6].

The European Parliament has endorsed draft measures to accelerate the rate of building renovations and minimize energy consumption and CO2eq emissions from buildings. These targets have been legally enshrined in the European Climate Law, making them binding obligations under European legislation [7]. According to the approved measures, all new buildings will need to be zero-emission buildings (ZEBs) by 2028. According to the approved measures, by 2028, all newly built buildings must be zero-emission buildings (ZEBs). Additionally, new buildings owned or used by public authorities should meet this requirement by 2026 [8], surpassing the standards set by nZEBs.

In the construction industry, lightweight steel frame (LSF) structures have continued to gain momentum in recent years. The advantages of LSF structures over traditional concrete and masonry structures include reduced weight, faster construction time, high potential for recycling and reuse, and lower greenhouse gas emissions over the building lifetime [9–14].

One of the major drawbacks of LSF elements is the increased risk of thermal bridging due to the use of thermally conductive materials such as steel [15–19]. For this reason, an emphasis should be placed on the analysis of thermal bridging and water vapor diffusion. Due to the more pronounced effect of thermal bridges, LSF elements require more thermal insulation to achieve minimal requirements set by the different standards in terms of U-values.

Another issue with LSF elements is quality control after the building is completed. Some quality control methods mostly used in practice are infrared thermography (IRT) [20,21] and the heat flow meter method (HFM). These methods can be used to determine surface temperatures and heat flows on site to verify the extent of thermal bridges and calculate the actual energy consumption.

One of the most important parameters in building energy consumption assessment is the thermal transmittance or U-value of each building component. The main method for determining the U-value is described in the ISO 6946 standard [22]. This standard contains methods for calculating the U-value of both homogeneous and inhomogeneous building elements, i.e., building elements with embedded load-bearing structure such as LSF elements.

Other methods for determining U-values include experimental and numerical methods. Experimental methods such as the protected heater box method according to the ISO 8990 standard [23] can be used in the laboratory to determine the steady-state U-value

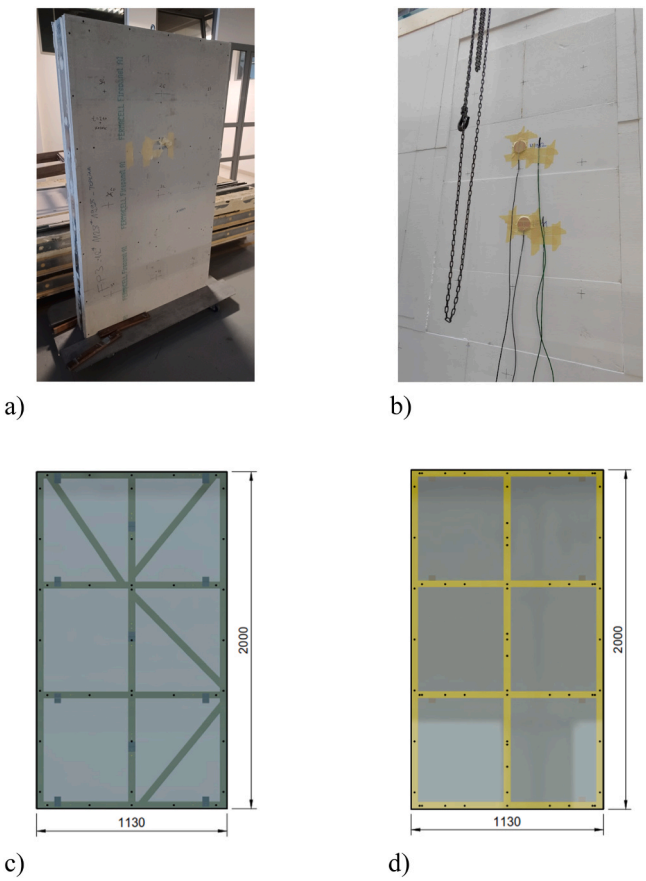

Fig. 1. Examined wall segments, (a) Hotbox sample, (b) EPS reference sample (RS-EPS), (c) With diagonal stiffeners, (d) Without diagonal stiffeners.

of the entire building element [24], while other methods such as the heat flux meter (HFM) method [25] according to the ISO 9869–1 standard and the infrared thermography (IRT) method [26] according to the ISO 9869–2 standard can be used in the field to verify the performance of the installed building elements [20,27–30]. Numerical methods as defined in the ISO 10211 standard [31] can be two- or three-dimensional, but require the use of specially designed thermal bridge numerical analysis software, such as AnTherm [32], Flixo [33], CRORAL [34], Therm [35], or other numerical thermal analysis software that passes the ISO 10211 and ISO 10077–2 reference tests [31]. Numerical methods are among the most accurate methods for determining the thermal bridge effect [13,17,24,27,28,36–39], but due to the sometimes complex geometries of structural elements, especially in the case of windows and LSF walls, and the need for higher computational power, their application is not very common in practice.

Since the presence of steel columns in LSF elements causes a higher heat transfer rate and more profound structural thermal bridges, it is a general rule that higher dimensional heat transfer calculations are required [19,40,41]. The objective of this work is to compare different methods for calculating the total U-value of the element – experimental, numerical, and analytical methods – and to see which of these methods can be used for calculating the U-value in the case of LSF elements.

Another objective of this work is to highlight the effect of the lightweight steel structure on the surface heat flux, especially for the HFM method since the location where the heat flow meter sensor is placed has a great influence on the measured U-value.

2. Wall samples description

Four different wall segments (Fig. 1a) and one EPS reference sample (Fig. 1b) were tested (Table 1). The wall samples consisted of a steel structure filled with polyurethane foam and a double and triple cladding of fire protection panels. An EPS reference sample with known thermal conductivity was tested to validate the test results. Fig. 2.

The load- bearing structure of the tested wall segments consists of steel C-sections with and without diagonal stiffeners (Fig. 1c and d). Two different wall thickness were examined because the examined samples were optimized for better sound insulation with additional fireboard panels on both sides of the sample. The thickness of the wall segments is 185 and 210 mm respectively, and the thickness of the reference sample is 185 mm. The overall external dimensions of all samples were 1130 × 2000 mm (width × height) (Table 2).

3. Experimental setup

3.1. Hotbox method

All samples described in Section 2 were tested in the hotbox chamber according to the ISO 8990 standard. The setup consists of one hot and one cold climatic chamber and a movable steel frame used for the installment of the test samples (Fig. 3a and b). A total of 18 thermocouples were attached to each sample to measure the surface temperature (9 on the cold side and 9 on the hot side) (Fig. 3c). Six additional thermocouples were used to measure air temperature, three on each side of the chamber, and six thermocouples were used to measure the surface temperature of the chamber screen parallel to the tested surfaces. All data acquisition was done with an automated system centrally controlled by software.

The adiabatic boundary condition about the perimeter of the sample was approximated by EPS with the same thickness as the samples and known thermal conductivity.

Thermocouples were placed on the surface of the tested samples near the steel studs to capture the effects of three-dimensional heat flow, and further away from the steel studs where the heat flow can be assumed as one-dimensional.

After installing the sample and test equipment, the environment on both sides of the sample is heated/cooled to reach 20 °C on the hot side and 0 °C on the cold side. The sample is held at these temperatures for 36 h. Air temperatures, surface temperatures, relative humidity and air velocities were measured during the measurement period. The hot side of the chamber is heated with a heating coil and fan that blows hot air over the tested surface. The cold side of the chamber is cooled with a split system air conditioners.

3.2. Heatflow method

The heat flow method (HFM) is used for in-situ determination of U-value by simultaneous measurement of heat flow with a flowmeter and indoor and outdoor temperature with a pair of thermocouples (Fig. 4) according to the ISO 9869 standard. Generally, the heat flux is averaged over a long-enough period of time to compensate for the daily variations in air temperature and heat flux over the area under the examined surface. If the heat flux and temperatures are semi-stationary during the measurement, the measurement

Table 1
Sample name and description.

Sample name	Sample description
W1-DS	d = 185 mm, with diagonal stiffeners and with two fireboards on both sides.
W1	d = 185 mm, without diagonal stiffeners and with two fireboards on both sides.
W2-DS	d = 210 mm, with diagonal stiffeners and with three fireboards on both sides.
W2	d = 210 mm, without diagonal stiffeners and with three fireboards on both sides.
RS-EPS	d = 185 mm, EPS with known thermal conductivity.

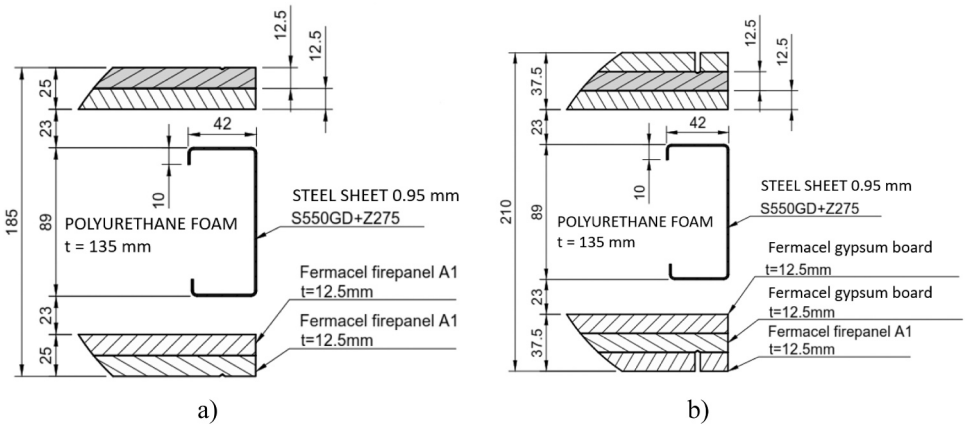

Fig. 2. Cross-sections, (a) W1-DS and W1, (b) W2-DS and W2.

Table 2
Thermal characteristics and thickness of the used materials.

Material	Thermal conductivity [W/ (m K)]	Thickness [mm]
Polyurethane foam	0.036	135
Fireboard	0.38	12.5
Steel	50.0	89
EPS	0.0326 ± 0.0010	185

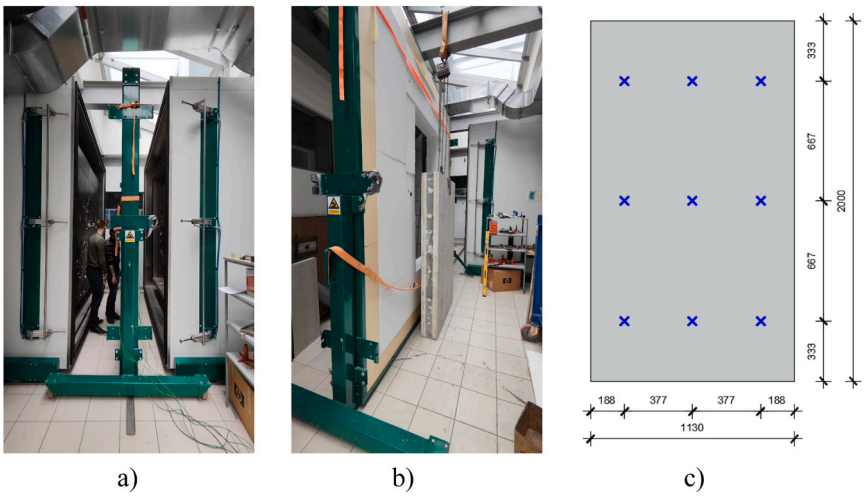

Fig. 3. Hotbox apparatus, (a) hot and cold chamber, (b) hotbox sample, (c) thermocouples position.

time can be shortened, as is the case in this research. The equipment used in this work is the TRSYS01 heat flux measurement system from Hukseflux, whose specifications (Table 3) meet all the requirements of the ISO 9869 standard.

The heat flow sensors were positioned on the surface of the warmer side of the samples, whereas the thermocouples measuring the internal and external air temperature were placed on both sides of the samples (two on the warmer side and two on the colder side). Fig. 5 shows the placement of the heat flow meter sensors for wall without diagonal stiffeners and the overlap with the load bearing structure. The exact location of the heat flux sensors for each sample is shown in Fig. 6.

Measurement aimed to determine the maximum heat flux at the junction of 6 steel studs and the minimum heat flux at the point where there are no studs but only a cross-section with polyurethane foam.

Heat flux and temperatures were measured over a 36-hour period, from which the average values of the heat flux and air temperatures were calculated. The average method of the ISO 9869 standard was used for the analysis. According to the average method, the U-value is calculated as follows:

Fig. 4. Heatflow meter apparatus, (a) TRSYS01 system, (b) heat flux sensor.

Table 3
Heatflow system specifications.

Measurement range	-2000 to + 2000 W/m^2
Sensitivity	60.77/61.68 μV/(W/m^2)
Sensor thermal resistance	71 × 10^{-4} K/(W/m^2)
Sensor thickness	5.4 mm
Uncertainty of calibration	±3% (k = 2)
Rated operating temperature range	-30 to + 70 °C
Acceptance interval temperature difference measurement	±0.1 °C

Fig. 5. Installation of the heatflow meter apparatus, (a) hot side, (b) cold side.

$$U = \frac{\sum_{i=1}^{n} q_i}{\sum_{i=1}^{n} \left(T_{\text{int}}^{i} - T_{ext}^{i}\right)} \tag{1}$$

In the equation (1), q_i represents the heat flux density in W/m^2, T_{int} and T_{ext} represent the internal and external air temperature in °C, respectively, and n indicates the total number of measurement points utilized to compute the average values.

4. Numerical simulations

4.1. Boundary conditions

Surface resistances were calculated according to ISO 8890 standard for each tested sample (Table 4). Different values of surface resistances for each sample are the result of different air velocities on both sides of the samples.

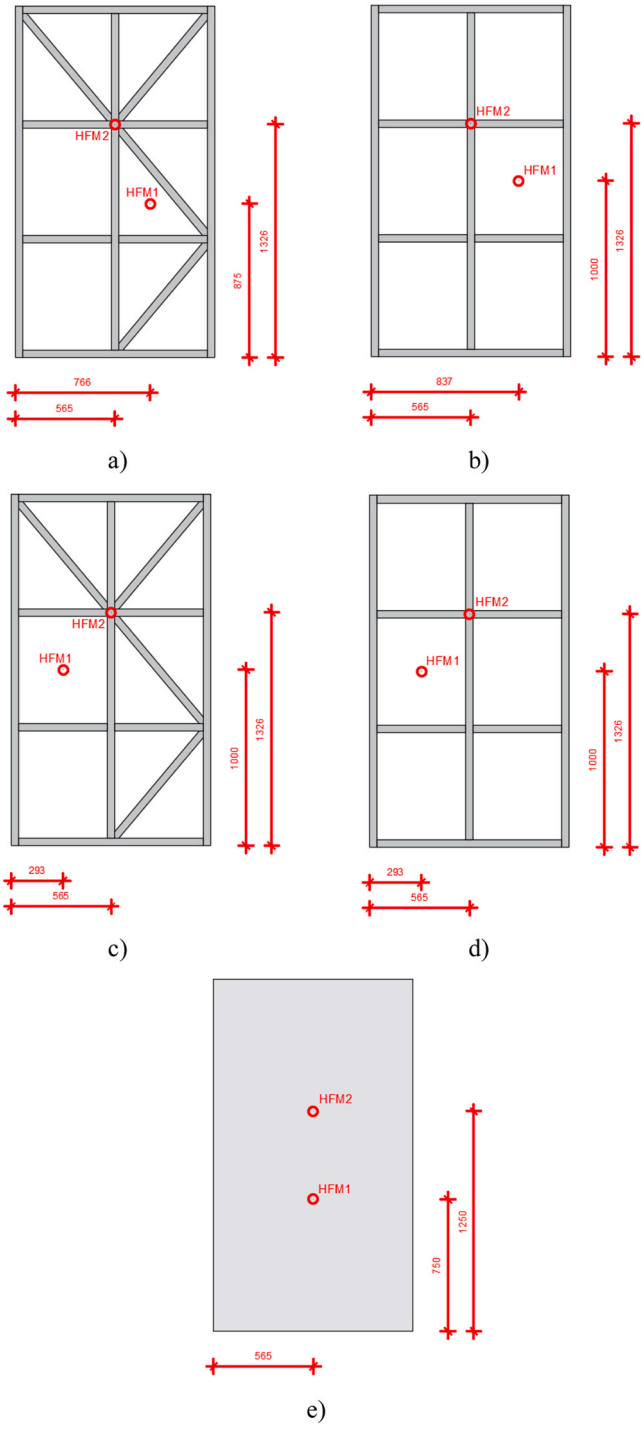

Fig. 6. Heat flux sensor location, (a) W1-DS, (b) W1, (c) W2-DS, (d) W2, (e) RS-EPS.

4.2. 3D numerical simulation

The three-dimensional thermal calculations were performed in AnTherm, a software specialized in the calculation of heat loss in building physics. Geometric models consist of the steel structure filled with polyurethane foam and all one-dimensional layers (fireboard and polyurethane foam), as shown in Fig. 7. The geometric models did not take into account the spacer between the steel structure and the fireboard plate, or the holes in the steel structure that serve to homogenize the polyurethane foam across the sample

Table 4
Surface resistances.

Sample name	Internal heat transfer coefficient R_{si}	External heat transfer coefficient R_{se}
	$(m^2 K)/W$	$(m^2 K)/W$
W1-DS	0.07	0.04
W1	0.05	0.06
W2-DS	0.11	0.05
W2	0.11	0.05
EPS reference sample	0.08	0.04

Boundary condition temperature used for the calculation were 20 °C on the hot side and 0 °C on the cold side.

volume.

AnTherm uses the control volume method (CVM) to calculate the unknown temperatures in the numerical grid. The temperatures are calculated for the center of each finite volume. Two different grid sizes were used for the calculation, one for the Samples 1–4 and one for submodels. Different grid sizes were used to show the accuracy of the numerical analysis for coarse and fine mesh. For Samples 1–4 the grid size was 25–50 mm with 25 mm step growth and for submodels the mesh size was 6–50 mm with 6 mm step growth. Another reason for coarse mesh size for Samples 1–4 is due to the limitation of software of 300000 cells for system of equations. Since the numerical calculations are done for a steady state heat transfer they can be done in matter of minutes on a personal computer that meets software requirements. The bigger problem is the limitation of the software to 300000 cells which leads to limitations in the mesh size.

To validate the results of the 3D calculation four different submodels were made for the samples with diagonal stiffeners (W1-DS and W2-DS) to validate coarse mesh used for the whole 3D model (Fig. 8).

The most important parameter of the 3D numerical calculation is the thermal coupling coefficient L_{3D} in W/K. In this case, L_{3D} is calculated as the total heat flux transferred through the cross-section dividing the two environments. If L_{3D} is known, then the U-value is calculated as:

$$U = \frac{L_{3D}}{A} \tag{2}$$

Where A is the area of the sample in m^2.

4.3. 2D numerical simulation

Because of complexity of 3D calculations in term of geometry and tools needed for the numerical calculation [19,40], another approach to calculating total heat flux without a 3D numerical calculation is to assume that total heat flux is the sum of 1D heat flux, 2D heat flux (linear thermal bridges), and in general case, 3D heat flux (point thermal bridges):

$$Q_{total} = Q_{1D} + Q_{2D} + Q_{3D} \tag{3}$$

$$Q_{1D} = U_{1D} \bullet A$$

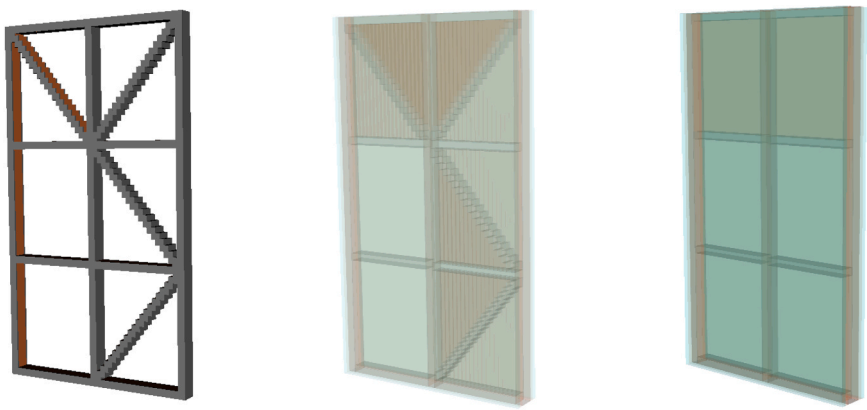

Fig. 7. Geometrical models, (a) Steel structure, (b) With diagonal stiffeners, (c) without diagonal stiffeners.

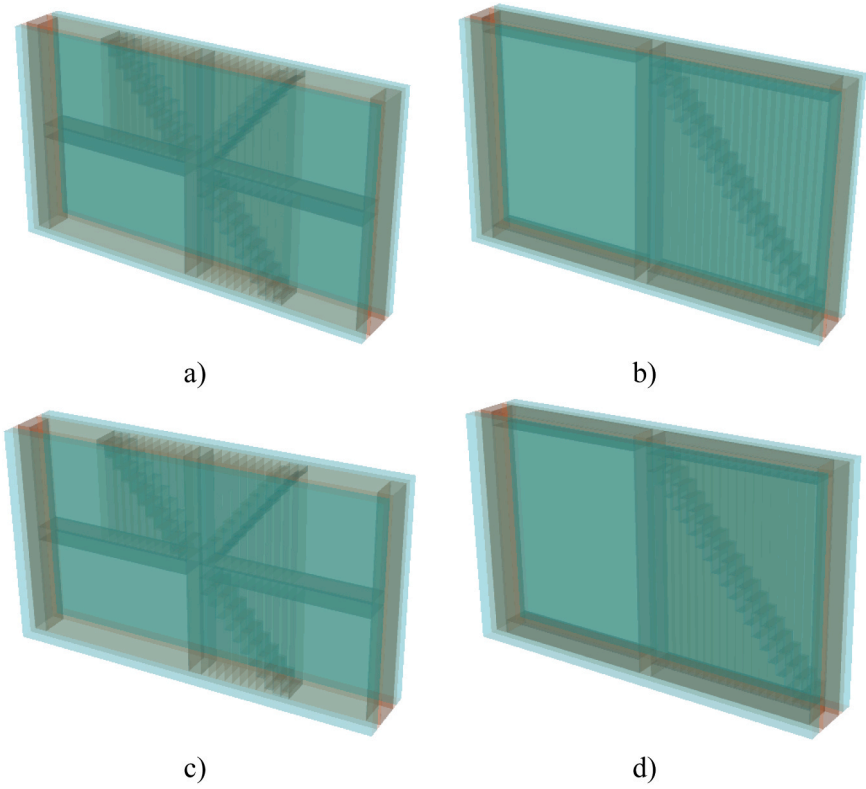

Fig. 8. Submodels, (a) W1-DS (junction), (b) W1-DS (stiffener), (c) W2-DS (junction), (d) W2-DS (stiffener).

$$Q_{2D} = \sum_{i=1}^{N} \psi_i \bullet L_i$$

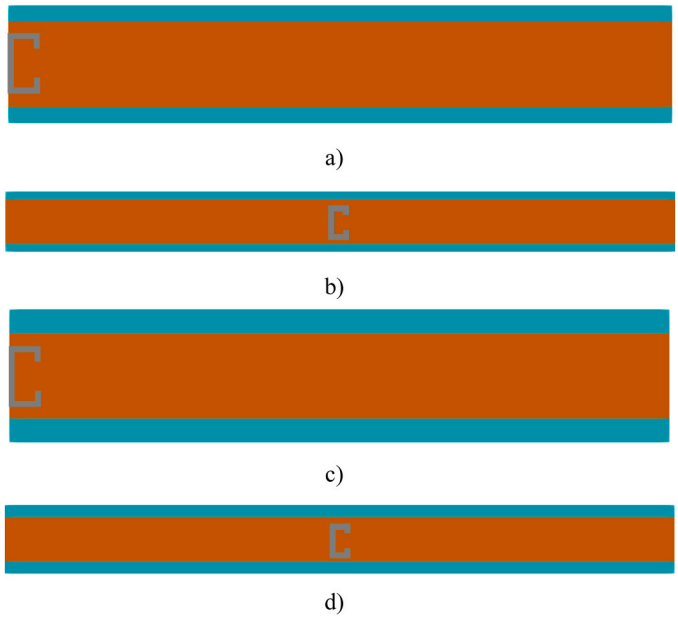

Fig. 9. Geometrical models for 2D numerical calculations, (a) W1-DS and W1 (TM1), (b) W1-DS and W1 (TM2), (c) W2-DS and W2 (TM1), (d) W2-DS and W2 (TM2).

$$Q_{3D} = \sum_{i=1}^{N} \chi_i$$

Where U_{1D} is the 1D thermal transmittance of the whole sample in W/(m^2 K), A is the surface area of the sample in m^2, ψ is the linear thermal transmittance in W/(m K), L is the thermal bridge length for which the ψ-value applies in m and χ is the point thermal transmittance in W/K.

Numerical calculations for 2D heat transfer were performed using CRORAL software. This software uses the same method as AnTherm to calculate the unknown temperatures (Control Volume Method).

ψ-value is calculated as the difference between the 2D heat flux (or L_{2D}) and 1D heat flux as follows:

$$\psi = L_{2D} - \sum_{j=1}^{M} U_j \bullet L_j \tag{4}$$

If the influence of 3D thermal bridges is ignored in the calculation, then the U-value is calculated as:

$$U_{sample} = \frac{U_{1D} \bullet A + \sum_{i=1}^{N} \psi_i \bullet L_i}{A} \tag{5}$$

The aim of this calculation is to test how ignoring the effect of point thermal bridges on the U-value compares to 3D numerical calculations and experimental methods.

A two-dimensional calculation is performed for all thermal bridges that affect the U-value. All 2D thermal bridges for all 4 samples can be reduced to 4 geometric models (Fig. 9 and Fig. 10), but since all 4 samples have different surface resistances, these results in 8 different numerical calculations.

ψ-value is calculated using external dimensions by procedure given in ISO 10211.

5. U-value calculation using analytical approach

The method most commonly used in practice to calculate the design U-value of LSF walls is the method described in the ISO 6946 standard for structural members with non-uniform layers. This method is based on a simplified procedure for calculating the thermal resistance of inhomogeneous building components. The method is applicable when the ratio between the upper and the lower limit of thermal resistance is less than 3/2. The total thermal resistance of a wall component is calculated as:

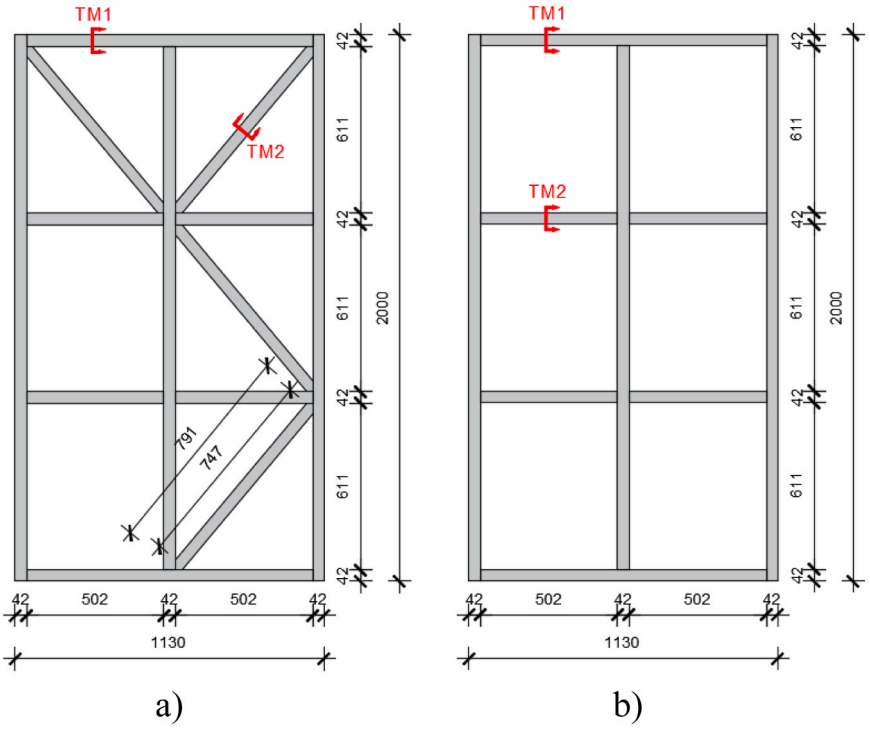

Fig. 10. 2D thermal bridges schemes and lengths, (a) W1-DS and W2-DS, (b) W1 and W2.

$$R_{tot} = \frac{R_{tot,upper} + R_{tot,lower}}{2}$$

$$U_{tot} = \frac{1}{R_{tot}} \tag{6}$$

Where R_{tot} is the total thermal resistance in (m^2 K)/W, $R_{tot,upper}$ and $R_{tot,lower}$ are the upper and lower limits of the total thermal resistance and U_{tot} is the total U-value in W/(m^2 K).

5.1. Upper limit calculation

The upper limit is calculated by assuming the 1D heat flow through the surface of the component (Fig. 11):

$$\frac{1}{R_{tot,upper}} = \frac{f_a}{R_{tot,a}} + \frac{f_b}{R_{tot,b}} + \ldots + \frac{f_o}{R_{tot,o}} \tag{7}$$

In the Eq. (7), $R_{tot,a}$, $R_{tot,b}$ and $R_{tot,o}$ represent the overall thermal resistances from one environment to another for each 1D segment, while f_a, f_b and f_o denote the respective fractional areas of each segment.

Upper U-value limit is calculated for W1-DS using Eq. 2 (Table 5) where L_i are the dimensions shown in Fig. 12 for each part of the cross section.

5.2. Lower limit calculation

The minimum threshold is computed by assuming that all layers within the component are uniform in temperature. However, when accounting for individual non-uniform layers to establish the equivalent thermal resistance for each of them, the thermal resistance is calculated as follows:

$$\frac{1}{R_j} = \frac{f_a}{R_{j,a}} + \frac{f_b}{R_{j,b}} + \ldots + \frac{f_o}{R_{j,o}} \tag{8}$$

Where R_j is the equivalent thermal resistance of the inhomogeneous layer "j" and $R_{j,a}$, $R_{j,b}$ and $R_{j,q}$ are the thermal resistances of each part of the inhomogeneous layer denoting to fractional surfaces f_a to f_o (Fig. 12).

When all the equivalent thermal resistances of the component are known the lower limit is calculated as:

$$R_{tot,lower} = R_{si} + R_a + R_b + \ldots + R_o + R_{se} \tag{9}$$

Lower U-value limit is calculated for W1-DS using Eq. 2 (Table 6) where L_i are the dimensions shown in Fig. 13 for each part of the cross section. Surface resistances are taken from Table 4.

5.3. Total analytical U-value

By using the same procedure for the calculation of upper and lower U-value limit for all LSF samples, analytical U-values for all four samples are calculated as the mean value between the upper and lower value (Table 7).

6. Results

6.1. Thermal transmittance (U-values)

6.1.1. Hotbox results

Results of the hotbox testing are measured heat fluxes and interior and exterior temperatures as shown in Table 8.

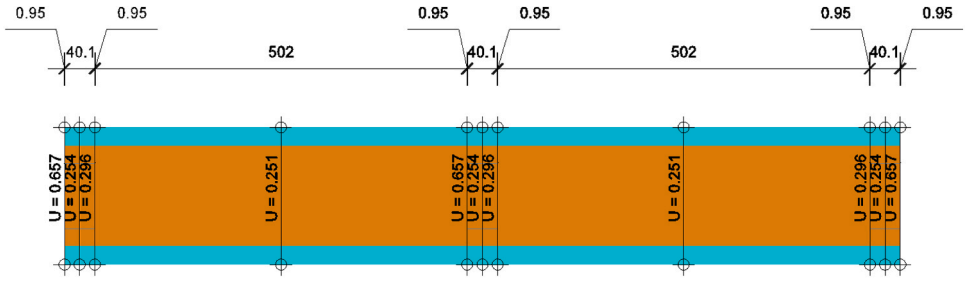

Fig. 11. Example of dimensions and 1D U-values used for the calculation of the upper limit (W1-DS).

Table 5
Upper U-value limit for analytical approach (W1-DS).

Cross section	U	R	L	f	f/R
	W/ (m^2 K)	(m^2 K)/W	mm	–	(m^2 K)/W
a	0.657	1.522	0.950	0.001	0.001
b	0.254	3.937	40.100	0.035	0.009
c	0.296	3.378	0.950	0.001	0.000
d	0.251	3.984	502.000	0.444	0.112
e	0.657	1.522	0.950	0.001	0.001
f	0.254	3.937	40.100	0.035	0.009
g	0.296	3.378	0.950	0.001	0.000
h	0.251	3.984	230.000	0.204	0.051
i	0.657	1.522	0.950	0.001	0.001
j	0.254	3.937	40.100	0.035	0.009
k	0.296	3.378	0.950	0.001	0.000
l	0.251	3.984	230.000	0.204	0.051
m	0.296	3.378	0.950	0.001	0.000
n	0.254	3.937	40.100	0.035	0.009
o	0.657	1.522	0.950	0.001	0.001
$1/R_{tot,upper} = 0.253$ W/(m^2 K)					

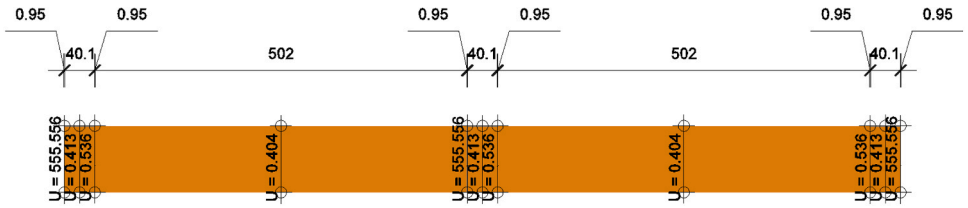

Fig. 12. Example of inhomogeneous layer dimensions and 1D U-values for the calculation of equivalent thermal resistance.

Table 6
Lower U-value limit for analytical approach (W1-DS).

Cross section	L	f	R = d/λ	f/R
	mm	–	(m^2 K)/W	(m^2 K)/W
a	0.950	0.001	0.002	0.472
b	40.100	0.035	2.419	0.015
c	0.950	0.001	1.864	0.000
d	502.000	0.444	2.472	0.180
e	0.950	0.001	0.002	0.472
f	40.100	0.035	2.419	0.015
g	0.950	0.001	1.864	0.000
h	230.000	0.204	2.472	0.082
i	0.950	0.001	0.002	0.472
j	40.100	0.035	2.419	0.015
k	0.950	0.001	1.864	0.000
l	230.000	0.204	2.472	0.082
m	0.950	0.001	1.864	0.000
n	40.100	0.035	2.419	0.015
o	0.950	0.001	0.002	0.472
$1/(R_{tot,lower} + R_{si} + R_{se}) = 0.511$ W/(m^2 K)				

6.1.2. HFM results

Table 9 shows the results of the HFM measurements. These results show the minimum and maximum heat fluxes and the average values of internal and external air temperatures, from which the minimum, maximum and average U-values are calculated using the average method as described in Section 3.2. Results of the measurement are shown in Fig. 13 together with the average U-values calculated for two different location (HFM1 and HFM2).

6.1.3. 3D numerical calculation

3D numerical calculation results are shown in Table 10 and Table 11, while Table 12 shows the difference between the L_{3D} thermal conductivity coefficient calculated for a coarse and a fine mesh. The maximum difference of 2.10% shows that the coarse mesh size is a good approximation for samples 1 and 3, which have diagonal stiffeners and are numerically more complex, i.e., a fine mesh would

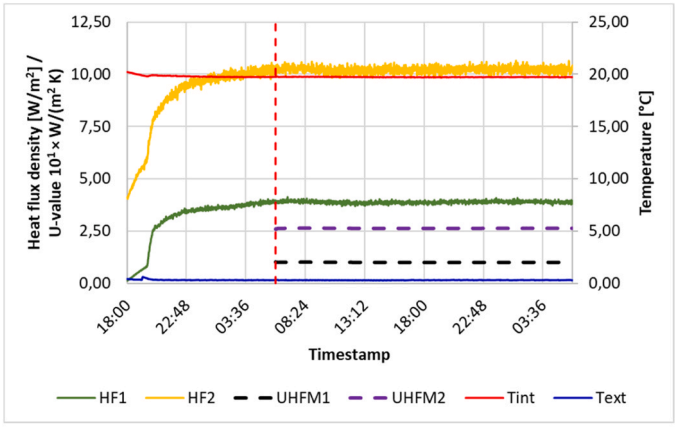

a)

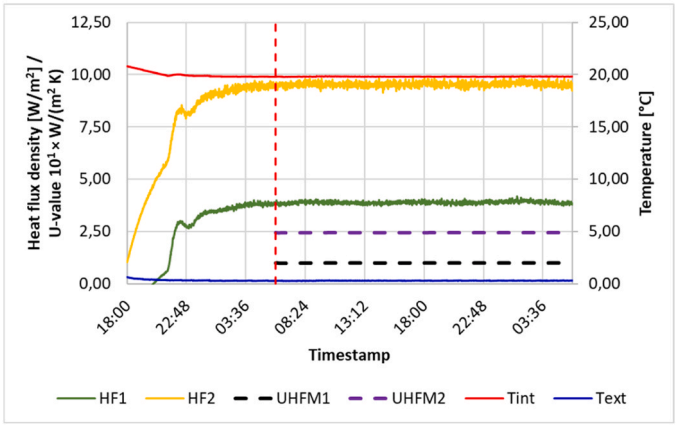

b)

Fig. 13. HFM measurement results (red dashed line is the beginning of average method), (a) W1-DS, (b) W1, (c) W2-DS, (d) W2, (e) RS-EPS.

result in a large system of equations that cannot be solved by AnTherm's solver.

For mesh sizes smaller than 5 mm, it becomes necessary to address the issue of point thermal bridges, a challenge encountered in the computational process. It should be emphasized that when using such fine mesh sizes, AnTherm's solver encounters difficulties in providing accurate results. Therefore, for the purpose of the numerical calculation in this research, these limitations have been taken into account and a coarse mesh was chosen for all numerical models for Samples 1–4 and more fine mesh was chosen for submodel numerical calculations.

The heat flux densities shown in Table 11 are calculated for the same location as the HFM method (Fig. 5), where q_1 corresponds to HFM1 and q_2 to HFM2 when stationary boundary conditions are achieved. The overall distribution of heat flux densities on the inner surfaces are shown in Fig. 14. A horizontal cross-section through the undisturbed section and the junction is shown in Fig. 15.

6.1.4. 2D numerical calculation

Results of the 2D numerical calculation are shown in Table 13 and Fig. 16. U-values are calculated by the procedure described in Section 4.3.

6.1.5. Verification of heatbox and HFM measurement

As mentioned in Section 2, an EPS reference wall sample was tested to validate the hotbox and HFM results. The wall sample consists of 185 mm thick EPS insulation with a known thermal conductivity of 0.0326 ± 0.0010 W/(m K) and a U-value of 0.171 ± 0.005 W/(m^2 K) calculated according to EN ISO 6946 for vertical walls. The U-values calculated by the hotbox and HFM methods are 0.173 and 0.181, respectively, which is less than 5% difference. Since the deviation of the design U-value (0.171) is about 3.2%, it is concluded that both the heatbox and HFM results outperform the reference measurement.

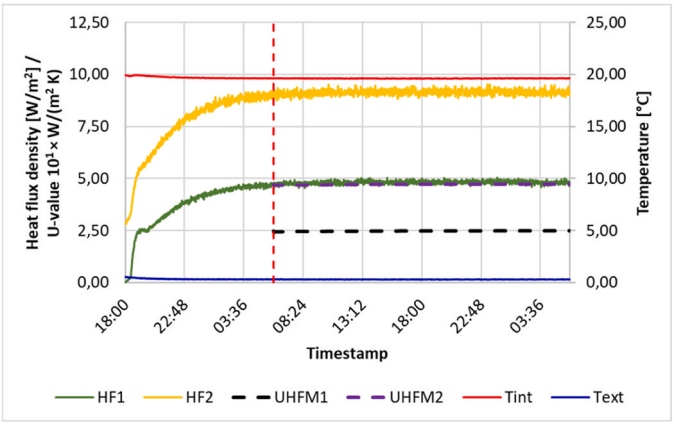

c)

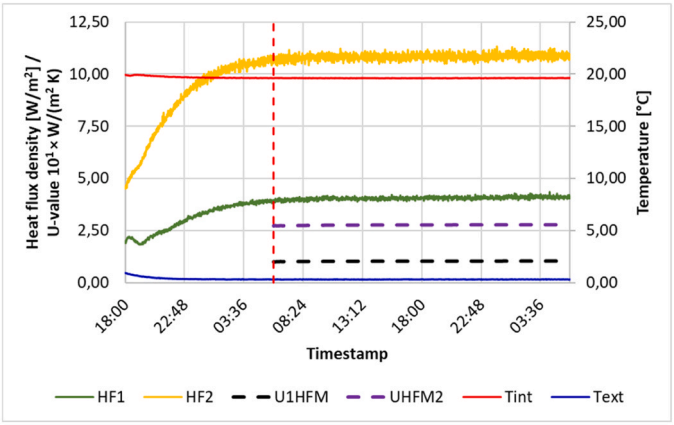

d)

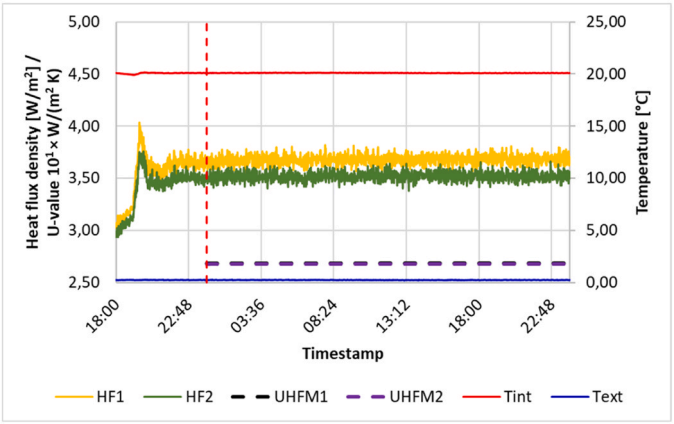

e)

Fig. 13. (*continued*).

6.1.6. *Comparison of results and discussion*

Fig. 17 through Fig. 20 show the comparison of results for all four different wall samples. Fig. 17 shows calculated U-values for all calculation methods, while Fig. 18 shows the difference between the calculated U-values compared to all calculation methods, respectively. Fig. 18 and Fig. 19 show the total and relative difference of the calculated heat flux densities.

Minimal and maximal differences between the calculated U-values are shown in Table 14. The maximum absolute difference for all

Table 7
Total U-value for analytical approach.

$U_{tot,lower}$	$U_{tot,upper}$	U_{tot}
W/(m^2 K)		
0.511	0.253	0.382
0.484	0.252	0.368
0.483	0.245	0.364
0.458	0.244	0.351

Table 8
Hotbox results.

Quantity	Unit	W1-DS	W1	W2-DS	W2	RS-EPS
q_{HB}	[W/m^2]	7.810	7.660	7.180	7.660	3.430
T_{int}	[°C]	20.260	20.32	20.210	20.210	20.00
T_{ext}	[°C]	0.500	0.510	0.490	0.510	0.410
U-value	[W/(m^2 K)]	0.395	0.387	0.364	0.364	0.173

Table 9
HFM results.

Quantity	Unit	W1-DS	W1	W2-DS	W2	RS-EPS
q_{HFM1}	[W/m^2]	3.883	3.887	4.815	4.052	3.677
q_{HFM2}	[W/m^2]	10.221	9.542	9.144	10.839	3.518
T_{int}	[°C]	19.734	19.817	19.618	19.814	20.104
T_{ext}	[°C]	0.298	0.290	0.310	0.304	0.236
U_{min}	[W/(m^2 K)]	0.200	0.199	0.249	0.208	0.185
U_{max}	[W/(m^2 K)]	0.526	0.489	0.474	0.556	0.177
U_{avg}	[W/(m^2 K)]	0.363	0.344	0.361	0.382	0.181

Table 10
Results of the 3D numerical calculation.

Quantity	Unit	W1-DS	W1	W2-DS	W2
L_{3D}	[W/K]	0.846830	0.768692	0.809656	0.737786
A	[m^2]	2.2600	2.2600	2.2600	2.2600
U-value	[W/(m^2 K)]	0.375	0.340	0.358	0.326

samples is 17.18% between the HFM and the 3D numerical calculation.

If hotbox and 3D numerical calculation results are compared, the maximum absolute difference is 13.82%. The maximum absolute difference between the calculated U-values is 6.15% between the 2D and the 3D numerical calculation.

Fig. 20 shows the comparison of heat flux between HFM and 3D numerical calculations for two locations shown in Fig. 5:

$$dq_1 = \frac{\left(q_{1,3D} - q_{1,HFM}\right)}{q_{1,HFM}} \tag{10}$$

$$dq_2 = \frac{\left(q_{2,3D} - q_{2,HFM}\right)}{q_{2,HFM}}$$

The maximum difference between the heat flux at the location without steel studs (q_{1HFM}) is 30.9%, while the difference between the heat flux at the junction of steel studs (q_{2HFM}) is 17.6%. If the HFM method is to be used to validate the design U-value of lightweight steel frame walls, the location for placing the HFM sensor is critical, as the difference between the heat fluxes q_{1HFM} and q_{2HFM} ranges from 90% to 167%. If the device is installed in a location where there is a steel stud, the result may be misleading. The measurement should only be performed if the stud placement scheme is known, and at least two heat flow meters should be used. One over the location without steel studs and one over the location with the maximum heat flux. In this work, the location with maximum heat flux is above the intersection of seven steel studs. The average of these two values is a good approximation of the final U-value, as shown in this research.

Fig. 21 shows the comparison of the analytically calculated U-value with the method described in the standard ISO 6946 (Section 5) and all other methods used in this research. The analytical U-value agrees well with the values determined both experimentally and numerically. The maximum absolute difference between the analytical U-value and all other methods is 8.83% for the HFM method.

Another aspect of this research was to show how numerical methods can be used to find the best location for placing the HFM

Table 11
Heat flux densities results of the 3D numerical calculation.

Quantity	Unit	W1-DS	W1	W2-DS	W2
q_1	[W/m^2]	5.230	4.970	4.880	4.930
q_2	[W/m^2]	11.540	10.710	10.990	9.160

Table 12
Submodel results of the 3D numerical calculation.

Quantity	Unit	Submodel 1	Submodel 2	Submodel 3	Submodel 4
$L_{3D,FM}$	[W/K]	0.281104	0.301362	0.273857	0.292941
$L_{3D,CM}$	[W/K]	0.275207	0.295757	0.268214	0.288084
ΔL_{3D}	**[%]**	**2.10**	**1.86**	**2.10**	**1.66**

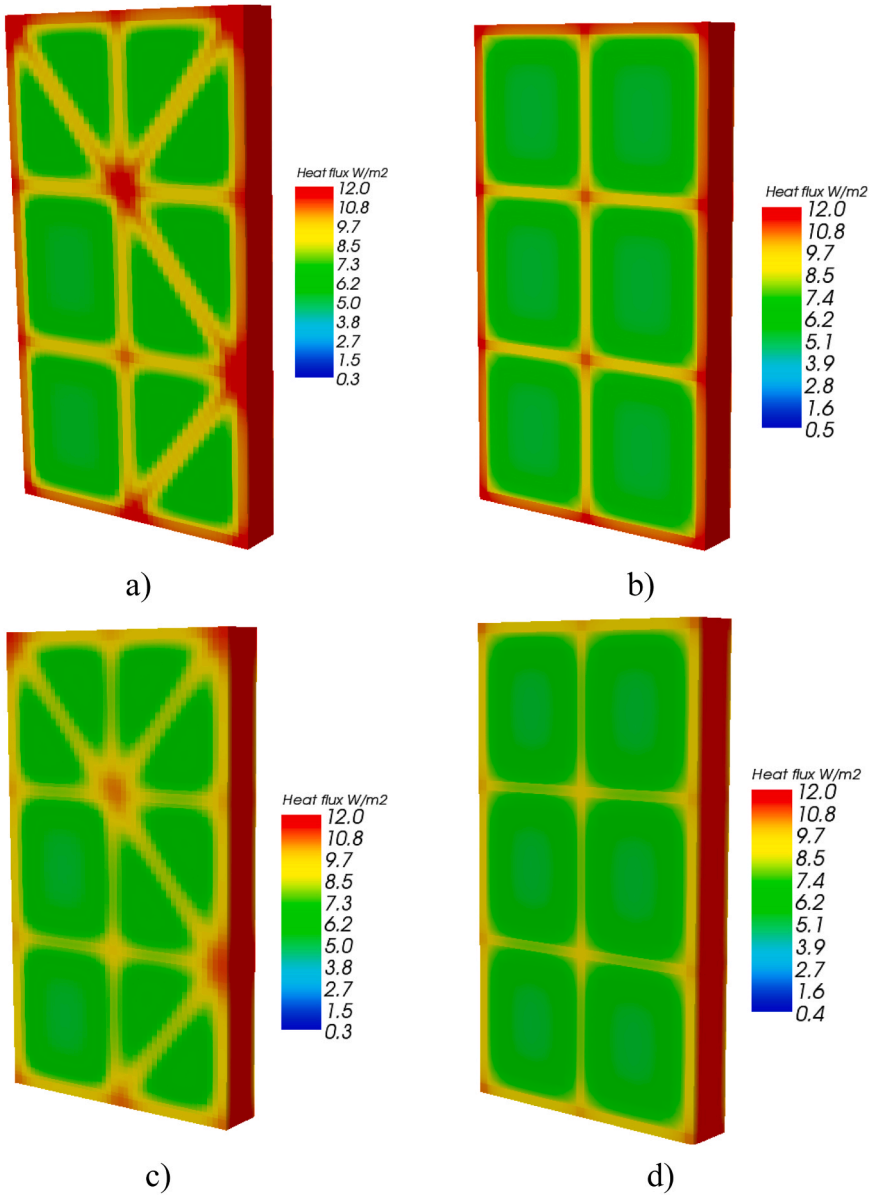

Fig. 14. Calculated surface heat flux density, (a) W1-DS, (b) W1, (c) W2-DS, (d) W2.

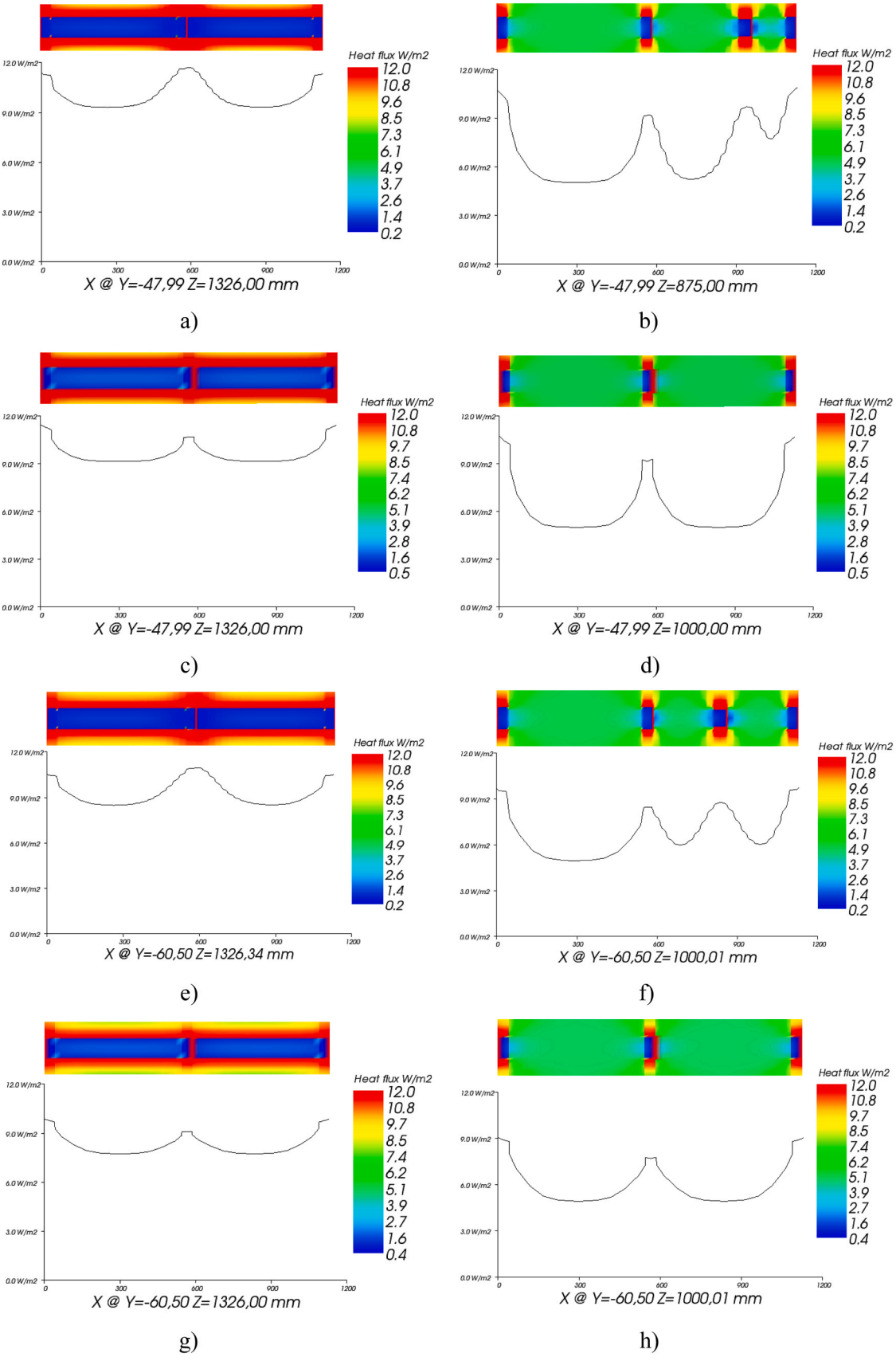

(caption on next page)

Fig. 15. Heat flux density profiles, (a) W1-DS (junction), (b) W1-DS (undisturbed heat flux), (c) W1 (junction), (d) W1 (undisturbed heat flux), (e) W2-DS (junction), (f) W2-DS (undisturbed heat flux), (g) W2 (junction), (h) W2 (undisturbed heat flux).

Table 13
Results of the 3D numerical calculation.

Quantity	Unit	W1-DS	W1	W2-DS	W2
Ψ_{TM1}	[W/(m K)]	0.020	0.020	0.019	0.019
$\sum L_{TM1}$	[m]	6.260	6.260	6.260	6.260
Ψ_{TM2}	[W/(m K)]	0.025	0.025	0.025	0.025
$\sum L_{TM2}$	[m]	7.660	4.260	7.660	4.260
U_{1D}	[W/(m^2 K)]	0.251	0.251	0.243	0.243
A	[m^2]	2.260	2.2600	2.260	2.260
U-value	[W/(m^2 K)]	0.391	0.354	0.380	0.343

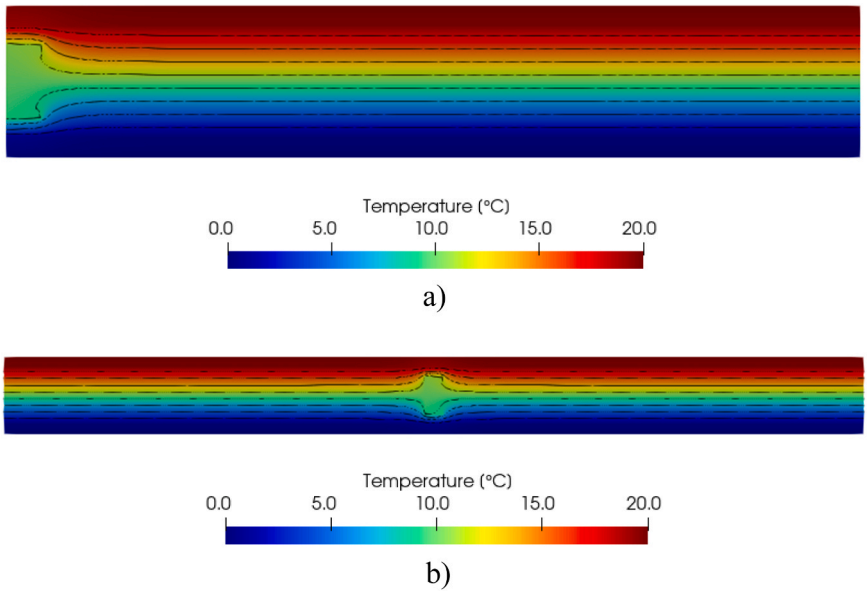

Fig. 16. Results of the 2D numerical calculation for W1-DS, (a) W1-DS (TM1), (b) W1-DS (TM2).

sensor. If one wants to accurately measure the U-value in situ then at least two heatflowmeter sensors should be used. One sensor should be placed at the location where the maximum heat flux is expected to occur. This location can be found either by examining the schematics of the installed steel framing or, if schematics are not known, by using nondestructive techniques such as infrared

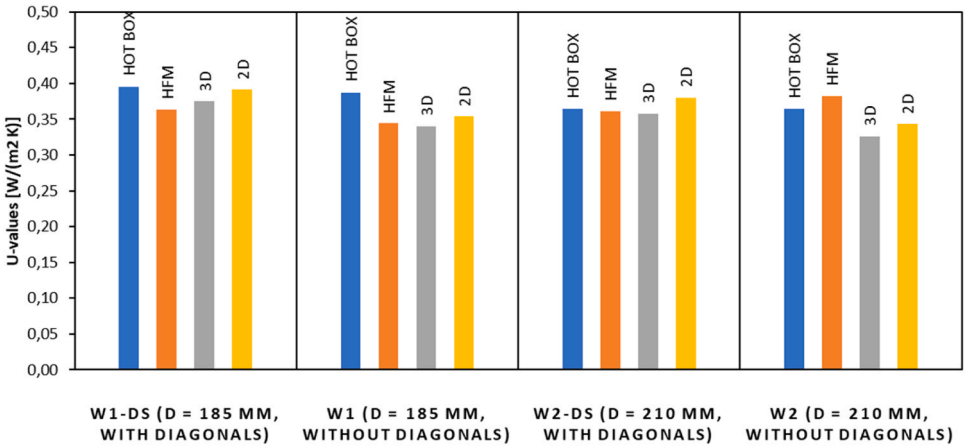

Fig. 17. Calculated U-values for all methods.

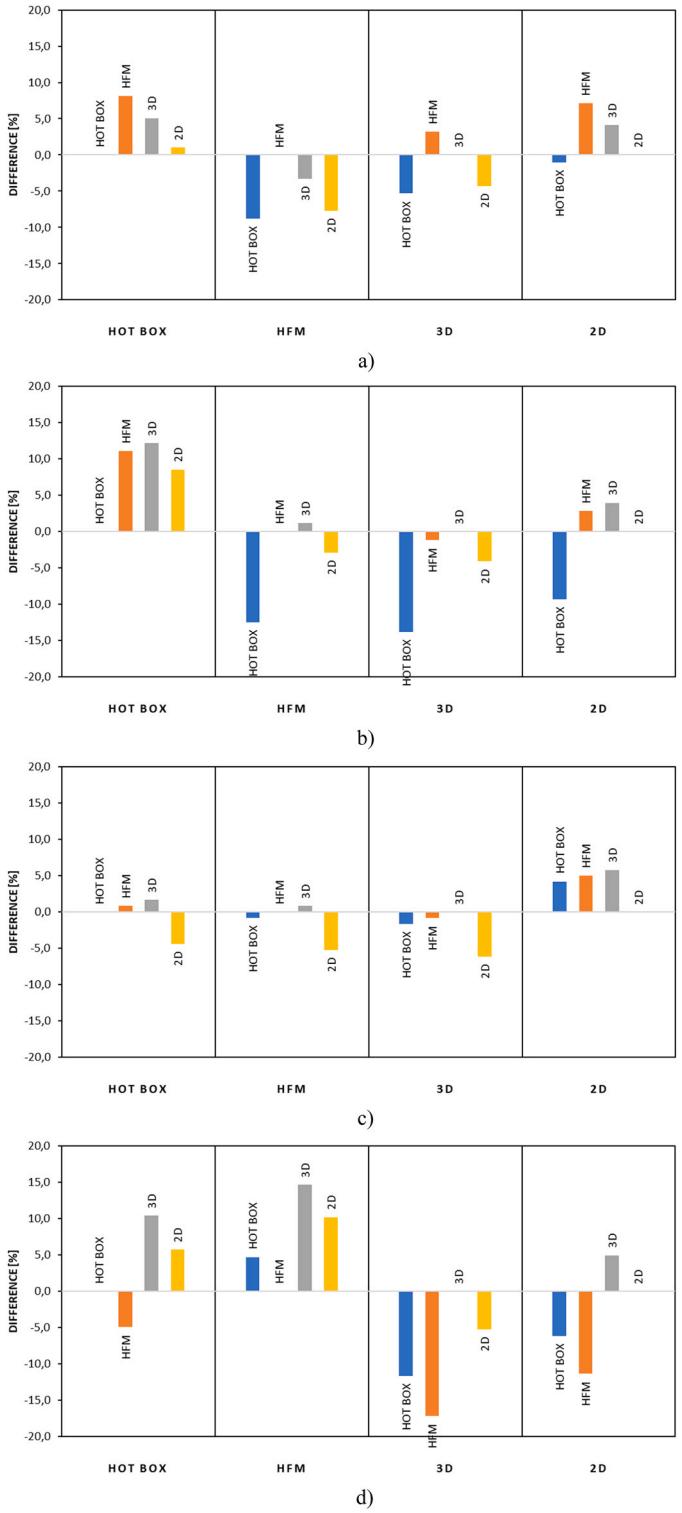

Fig. 18. U-value comparison for all methods, (a) W1-DS, (b) W1, (c) W2-DS, (d) W2.

thermography or rebar locators. The second sensor should be placed on the surface where the heat flow is considered to be one-dimensional. A good approximation of the total U-value of the LSF wall is the average of the maximum and minimum U-values, as shown in this research.

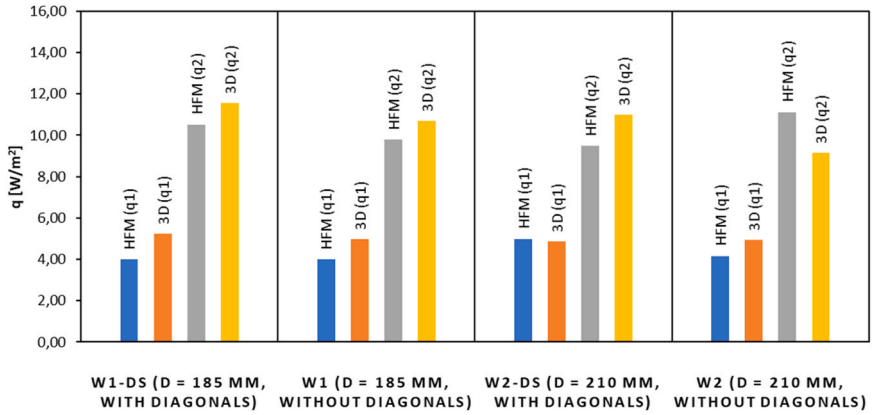

Fig. 19. Calculated heat flux densities for all methods.

Table 14
Minimal and maximal differences between calculation methods.

	Minimal difference [%]	Methods	Maximal difference [%]	Methods
W1-DS	1.01	2D/HOTBOX	-8.82	HOTBOX/HFM
W1	1.16	3D/HFM	-13.82	HOTBOX/3D
W2-DS	0.82	HFM/HOTBOX	-6.15	2D/3D
W2	4.71	HOTBOX/HFM	-17.18	HFM/3D

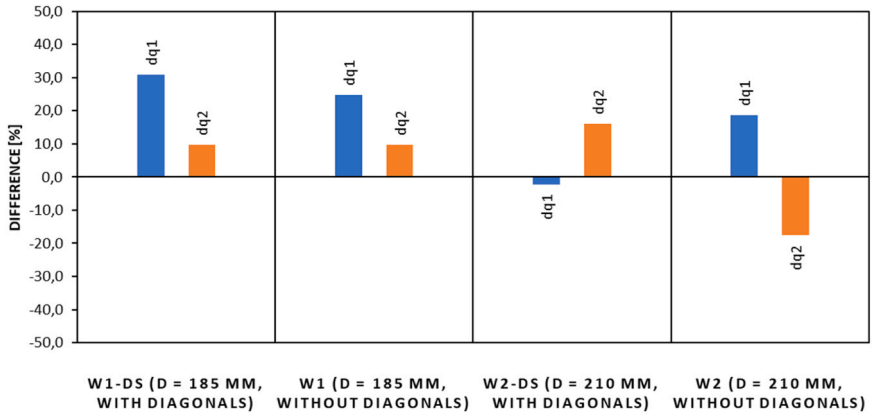

Fig. 20. Heat flux comparison for all methods.

7. Conclusion

Four different lightweight steel frame walls were experimentally tested alongside a reference wall made of EPS. Numerical calculations were conducted using AnTherm for 3D and CRORAL for 2D scenarios. The standard ISO 6946 was used for analytical approximation of the U-value. The main conclusions and new findings of this research are given below.

Objectives:

- The primary aim of this research was to compare U-values and surface heat fluxes obtained through various methods, including experimental, numerical, and analytical approaches.
- Secondary objective of this research was to, by comparing the results of the numerical and experimental results, give guidelines for calculating the U-value in-situ using the HFM method.

Experimental method comparison:

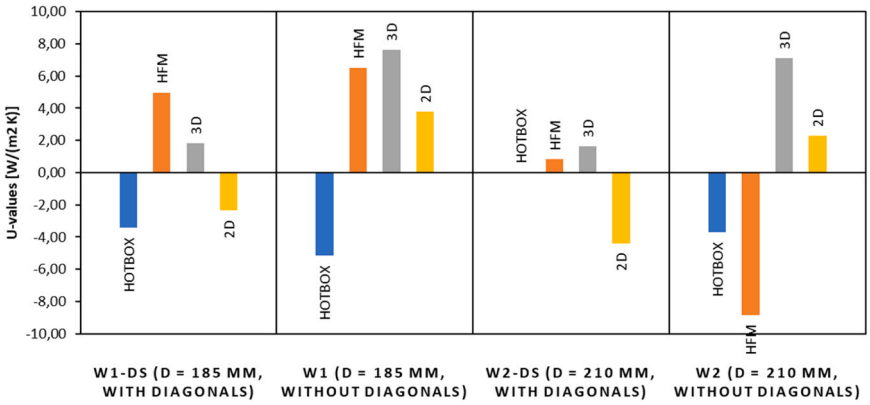

Fig. 21. Comparison of analytical U-value with experimental and numerical results.

- Both the hotbox and the HFM (Heat Flux Measurement) methods successfully passed a reference test, with a maximum U-value difference of less than 5% between them.

  3D vs. 2D numerical calculations:

- When comparing 3D and 2D numerical calculations for all four samples, the maximum absolute difference was found to be 6.15%.

  Efficiency of HFM method:

- The research demonstrated that the placement of HFM sensors for lightweight steel frame walls in-situ is crucial. The location should align with the steel frame installation scheme, as the difference in heat fluxes over the sample surface can be as high as 167%.

  Placement of the HFM sensors:

- One of the main conclusions in this research is that if HFM is to be used for determining the U-value of the LSF walls in-situ the following procedure should be used:

1. At least two HFM heatflowmeter sensors should be used.
2. First sensor should be placed on the location on the surface where the maximum heat flow is expected. This location can be found either by inspecting the schematics of the frame installation or by using the nondestructive technique such as infrared thermography or rebar locators to find the framework scheme.
3. Second sensor should be placed on the surface on the location where the heat flow is minimal, i.e. one-dimensional.
4. A good approximation of the Total U-value is the average of the maximal and minimal U-value calculated from heat flux densities 2 and 3 as shown in this research.

Analytical U-Values:

- Analytical U-values, as per ISO 6946, closely matched the values obtained experimentally and numerically, with a maximum difference of 8.83%.
- The analytical approach described in ISO 6946 can be considered a reliable reference point for designing U-values for polyurethane lightweight steel frame elements. This applies not only to simpler configurations but also to elements with more complex structural geometry, such as steel frames with diagonal stiffeners.

Declaration of Competing Interest

I acknowledge that the research conducted for this manuscript was partially funded by the EU project KK.01.1.1.07.0060, titled "Composite lightweight panel with integrated load-bearing structure (KLIK-PANEL)." This project provided financial support for the research activities, including data collection, analysis, and interpretation.

Data availability

Data will be made available on request.

Acknowledgements

This research was funded by the European Union through the European Regional Development Fund's Competitiveness and Cohesion Operational Program, grant number KK.01.1.1.07.0060, project "Composite lightweight panel with integrated load-bearing structure (KLIK-PANEL)".

References

[1] European Commission, In focus: Energy efficiency in buildings, n.d. ⟨https://commission.europa.eu/news/focus-energy-efficiency-buildings-2020–02-17_en⟩ (accessed on 23 June 2023).
[2] L.C. a M. Economidou a, V. Todeschi a b, P. Bertoldi a, D. D'Agostino a, P. Zangheri a, Review of 50 years of EU energy efficiency policies for buildings, 2020. https://doi.org/https://doi.org/10.1016/j.enbuild.2020.110322.
[3] European Commission, Energy performance of buildings directive, 2023. ⟨https://energy.ec.europa.eu/topics/energy-efficiency/energy-efficient-buildings/energy-performance-buildings-directive_en⟩ (accessed on 23 June 2023).
[4] European Parliament, BRIEFING Towards climate neutrality: Fit for 55 package, 2021.
[5] EU Monitor, The European Green Deal, 2019. ⟨https://www.eumonitor.eu/9353000/1/j9vvik7m1c3gyxp/vl4cnhyp1ort⟩ (accessed on 23 June 2023).
[6] EU Monitor, Annex to the communication from the commission to the european parliament, the european council, the council, the european economic and social committee and the committee of the regions The European Green Deal, 2019. ⟨https://www.eumonitor.eu/9353000/1/j9vvik7m1c3gyxp/vl4d8dfd2dye⟩ (accessed on 23 June 2023).
[7] European Commission, European Climate Law, Off. J. Eur. Union. 2021, 2021: 17. ⟨https://eur-lex.europa.eu/legal-content/EN/TXT/?uri=CELEX:32021R1119⟩.
[8] P.A. Fokaides, A. Kylili, I. Kyriakides, Boundary conditions accuracy effect on the numerical simulations of the thermal performance of building elements, Energies 11 (2018), https://doi.org/10.3390/en11061520.
[9] N. Soares, P. Santos, H. Gervásio, J.J. Costa, L. Simões, Energy e ffi ciency and thermal performance of lightweight steel-framed (LSF) construction: A review, 78, 2017: 194–209. https://doi.org/10.1016/j.rser.2017.04.066.
[10] D. Perera, I.R. Upasiri, K. Poologanathan, P. Gatheeshgar, P. Sherlock, T. Hewavitharana, T. Suntharalingam, Energy performance of fire rated LSF walls under UK climate conditions, J. Build. Eng. 44 (2021), 103293, https://doi.org/10.1016/j.jobe.2021.103293.
[11] M.J. Rukavina, D. Skejić, A. Kralj, T. Ščapec, B. Milovanović, Development of lightweight steel framed construction systems for nearly-zero energy buildings, Buildings 12 (2022), https://doi.org/10.3390/buildings12070929.
[12] B. Milovanović, M. Bagarić, M. Gaši, N. Vezilić Strmo, Case study in modular lightweight steel frame construction: thermal bridges and energy performance assessment, Appl. Sci. 12 (2022), https://doi.org/10.3390/app122010551.
[13] I.A. Atsonios, I.D. Mandilaras, D.A. Kontogeorgos, M.A. Founti, Two new methods for the in-situ measurement of the overall thermal transmittance of cold frame lightweight steel-framed walls, Energy Build. 170 (2018) 183–194, https://doi.org/10.1016/j.enbuild.2018.03.069.
[14] L. Kempton, G. Kokogiannakis, A. Green, P. Cooper, Evaluation of thermal bridging mitigation techniques and impact of calculation methods for lightweight steel frame external wall systems, J. Build. Eng. 43 (2021), 102893, https://doi.org/10.1016/j.jobe.2021.102893.
[15] P. Santos, P. Lopes, D. Abrantes, Thermal performance of lightweight steel framed facade walls using thermal break strips and ETICS: a parametric study, Energies 16 (2023), https://doi.org/10.3390/en16041699.
[16] P. Santos, D. Abrantes, P. Lopes, Experimental and numerical performance evaluation of bio-based and recycled thermal break strips in LSF partition walls, Buildings 12 (2022), https://doi.org/10.3390/buildings12081237.
[17] L. Moga, I. Petran, P. Santos, Thermo-energy performance of lightweight steel framed constructions: a case study, Buildings 1 (2022), https://doi.org/10.3390/buildings12030321.
[18] P. Santos, The importance of stud flanges size and shape on the thermal performance of lightweight steel framed walls, Sustainability 13 (2021) 1–22, https://doi.org/10.3390/su13073970.
[19] P. Santos, G. Lemes, D. Mateus, External Facade LSF Walls: A Parametric Study, Energies (2019) 1–20, https://doi.org/10.3390/en12142671.
[20] M. Gaši, B. Milovanović, S. Gumbarević, Comparison of infrared thermography and heat flux method for dynamic thermal transmittance determination, Buildings 9 (2019) 132, https://doi.org/10.3390/buildings9050132.
[21] A. François, L. Ibos, V. Feuillet, J. Meulemans, In situ measurement method for the quantification of the thermal transmittance of a non-homogeneous wall or a thermal bridge using an inverse technique and active infrared thermography, Energy Build. 233 (2021), https://doi.org/10.1016/j.enbuild.2020.110633.
[22] EN ISO 6946, Building components and building elements — Thermal resistance and thermal transmittance — Calculation methods, 2017.
[23] The International Organization for Standardization, ISO 8990:1994 Thermal insulation — Determination of steady-state thermal transmission properties — Calibrated and guarded hot box, 1994.
[24] P. Santos, G. Lemes, D. Mateus, Analytical methods to estimate the thermal transmittance of LSF walls: Calculation procedures review and accuracy comparison, Energies 13 (2020), https://doi.org/10.3390/en13040840.
[25] International Organization for Standardization, ISO 9869–1:2014 - Thermal insulation – Building elements – In-situ measurement of thermal resistance and thermal transmittance – Part 1: Heat flow meter method, 2014: 36. ⟨https://www.iso.org/standard/59697.html⟩ (accessed June 3, 2019).
[26] The International Organization for Standardization, ISO 9869–2:2018 Thermal insulation — Building elements — In-situ measurement of thermal resistance and thermal transmittance — Part 2: Infrared method for frame structure dwelling, 2018.
[27] P. Santos, D. Mateus, D. Ferrandez, A. Verdu, Numerical simulation and experimental validation of thermal break strips' improvement in facade LSF walls, Energies 15 (2022), https://doi.org/10.3390/en15218169.
[28] P. Santos, M. Gonçalves, C. Martins, N. Soares, J.J. Costa, Thermal transmittance of lightweight steel framed walls: Experimental versus numerical and analytical approaches, J. Build. Eng. 25 (2019), 100776, https://doi.org/10.1016/j.jobe.2019.100776.
[29] S. Gumbarević, B. Milovanović, M. Gaši, M. Bagarić, Application of multilayer perceptron method on heat flow meter results for reducing the measurement time †, Eng. Proc. 2 (2020) 1–6, https://doi.org/10.3390/ecsa-7-08272.
[30] S. Gumbarević, B. Milovanović, B. Dalbelo Bašić, M. Gaši, Combining Deep Learning and the Heat Flux Method for In-Situ Thermal-Transmittance Measurement Improvement, Energies 15 (2022), https://doi.org/10.3390/en15145029.
[31] The International Organization for Standardization, ISO 10211:2017 Thermal bridges in building construction — Heat flows and surface temperatures — Detailed calculations, 2017.
[32] Kornicki, An.Therm (Thermal Heat Bridges), 2023. ⟨http://www.antherm.at/⟩ (accessed on 23 June 2023).
[33] Infomind GmbH, The thermal bridge analysis and reporting application, 2023. ⟨https://www.flixo.com/⟩ (accessed on 23 June 2023).
[34] M. Gaši, CRORAL-Computer Program for Thermal Bridge Analysis and Vapour Analysis, 2023. https://www.croral.org/ (accessed on 23 June 2023).
[35] Windows and Daylighting, THERM, 2023. ⟨https://windows.lbl.gov/⟩ (accessed on 23 June 2023).
[36] M. Pomada, J. Adamus, A. Boruszewski, Numerical and experimental analysis of heat flow at window-to-wall interface, Energies 15 (2022), https://doi.org/10.3390/en15103837.
[37] M. Rahiminejad, D. Khovalyg, Numerical and experimental study of the dynamic thermal resistance of ventilated air-spaces behind passive and active façades, Build. Environ. 225 (2022), 109616, https://doi.org/10.1016/j.buildenv.2022.109616.
[38] R. Hart, Numerical and experimental validation for the thermal transmittance of windows with cellular shades, Energy Build. 166 (2018) 358–371, https://doi.org/10.1016/j.enbuild.2018.02.017.
[39] U. Berardi, T. Kisilewicz, S. Kim, A. Lechowska, J. Paulos, J. Schnotale, Experimental and numerical investigation of the thermal transmittance of PVC window frames with silica aerogel, J. Build. Eng. 32 (2020), 101665, https://doi.org/10.1016/j.jobe.2020.101665.
[40] E. Roque, P. Santos, The effectiveness of thermal insulation in lightweight steel-framedwalls with respect to its position, Buildings 7 (2017), https://doi.org/10.3390/buildings7010013.
[41] P. Santos, D. Abrantes, P. Lopes, D. Mateus, Experimental and numerical performance evaluation of bio-based and recycled thermal break strips in LSF partition walls, Buildings 12 (2022), https://doi.org/10.3390/buildings12081237.